Journal of Solid State Chemistry **149,** 414–418 (2000)
doi:10.1006/jssc.1999.8568, available online at http://www.idealibrary.com on IDEAL®

Synthesis and Crystal Structure of SrV_4O_9 in a Metastable State

Yoshio Oka,*,[1] Takeshi Yao,† Naoichi Yamamoto,‡ Miki Ueda,‡ and Satoru Maegawa‡

*Department of Natural Environment Sciences, Faculty of Integrated Human Studies, †Department of Fundamental Energy Sciences, Graduate School of Energy Sciences, and ‡Graduate School of Human and Environmental Studies, Kyoto University, Kyoto 606-8501, Japan

Received September 8, 1999; accepted November 5, 1999

In the $SrO–VO_2$ phase diagram there exists no SrV_4O_9 phase corresponding to the CaV_4O_9 phase in the $CaO–VO_2$ diagram and synthesis of SrV_4O_9 has not been reported so far. We are successful in hydrothermal synthesis of the synthesis of SrV_4O_9: hydrothermal treatment of $SrCl_2–NaVO_3–(CH_3)_4NCl$ solutions above 300°C yielded light-green plate crystals identified as SrV_4O_9. Single-crystal X-ray diffractometry confirmed the CaV_4O_9-type structure consisting of V_4O_9 layers and interstitial Sr atoms: $P4/n$, $a = 8.379(2)$ Å, $c = 5.259(3)$ Å, and $Z = 2$. The refinements based on 826 reflections with $I > 3\sigma(I)$ converged to $R = 0.039$ and $R_w = 0.048$. Temperature variation of magnetic susceptibility exhibits a low-dimensional feature of a broad maximum around 100 K, just like that of CaV_4O_9. Single crystals of CaV_4O_9 were similarly grown in the hydrothermal $CaCl_2–NaVO_3–(CH_3)_4NCl$ system at 280°C and its single-crystal X-ray study was also made to compare with those of SrV_4O_9. © 2000 Academic Press

***Key Words*: strontium vanadium oxide; hydrothermal synthesis; metastable phase; layered structure; low-dimensional spin system.**

INTRODUCTION

Vanadium oxide compounds with V^{4+} ($S = \frac{1}{2}$) ions have attracted much attention due to their possibility to adopt layer-type V–O polyhedral frameworks which inherently exhibit interesting low-dimensional magnetic behavior originating from $S = \frac{1}{2}$ spins. Their magnetic systems are classified into several groups such as spin ladder, spin plaquette, and dimer systems, depending on their structural and magnetic properties. Research interest has been accelerated by the discovery of the spin Peierls transition in α'-NaV_2O_5 by Isobe and Ueda (1). The low-dimensional magnetic properties of AV_2O_5 with layered structures for A = Na, Cs, Mg, Li were recently reviewed by Ueda (2). The spin plaquette system is attributed to other layered structures of AV_3O_7 for A = Ca(3), Sr(4), and AV_4O_9 for A = Ca(5), both of which have similar V–O layers consisting of edge-sharing VO_5 square pyramids whose structures look like tiling plaquettes of VO_4 square bases. The AV_4O_9 phase appears only for A = Ca, unlike the AV_3O_7 phase appearing for A = Ca, Sr (6, 7): according to the $SrO–VO_2$ phase diagram, the stoichiometric composition of SrV_4O_9 gives a two-phase state consisting of SrV_5O_{11} and SrV_3O_7 (6). However, SrV_4O_9 of the AV_4O_9 phase could possibly exist in a metastable state since SrV_3O_7 of the AV_3O_7 phase that is structurally related to the AV_4O_9 phase does exist.

There are several ways to reach metastable compounds: for example, high-pressure syntheses, soft chemical processes, and chemical vapor depositions. Hydrothermal synthesis is one of the soft chemical processes that produce metastable compounds (8–10) and has an advantage of giving single crystals suitable for structure determination. Typical examples are found in the hydrothermal synthesis of metastable VO_2 phases (11, 12). In the present study we have applied hydrothermal synthesis to the Sr–V–O system and succeeded in producing single crystals of metastable SrV_4O_9 of the CaV_4O_9 type. Single crystals of CaV_4O_9 were also hydrothermally grown in a similar manner and its crystallographic data are presented to compare with those of SrV_4O_9.

EXPERIMENTAL

Sample Preparation

Hydrothermal synthesis of SrV_4O_9 was carried out using a $SrCl_2–NaVO_3$ mixed solution to which tetramethyl ammonium chloride ($(CH_3)_4NCl$) was added as a reducing agent from V^{5+} to V^{4+}. An aqueous solution of 0.1 M $SrCl_2$, 0.1 M $NaVO_3$, and 0.02 M $(CH_3)_4NCl$ were sealed in a quartz ampoule followed by hydrothermal treatment at 350°C for 48 h. Precipitates consisting of red-brown powders and light-green plate crystals were filtered out; the former was larger in amount than the latter. The light-green crystals were separated by leaching the red-brown powders in dilute hydrochloric acid and subsequent ultrasonic purification. Powder X-ray diffraction of the light-green crystals

[1]To whom correspondence should be addressed. E-mail: oka@kagaku.h.kyoto-u.ac.jp. Fax: + 81-75-752-0703.

0022-4596/00 $35.00

showed an almost identical pattern to that of CaV_4O_9 (13), regardless of the peak positions at slightly lower 2θ angles. A crystalline phase of the red-brown powders was identified to be $Sr_2V_3O_9$ (6, 14). An EDX analysis on the light-green crystals gave an atomic ratio of $Sr/V = \frac{1}{4}$. Consequently, the light-green crystals are surely a new compound, SrV_4O_9. Single crystals of CaV_4O_9 were similarly obtained by the hydrothermal treatment of an aqueous solution of 0.1 M $CaCl_2$, 0.1 M $NaVO_3$, and 0.02 M $(CH_3)_4NCl$ at 280°C for 48 h, where CaV_3O_7 crystals were sometimes included as a minor product. Magnetic susceptibility was measured on refined SrV_4O_9 crystals by using a SQUID magnetometer.

Single-Crystal X-Ray Diffraction

A single-crystal X-ray diffraction study was made on both SrV_4O_9 and CaV_4O_9 crystals. Selected crystals were mounted on a Rigaku AFC-7R X-ray diffractometer with monochromatized Mo$K\alpha$ radiation. Diffraction data were collected by the 2θ–ω scanning method and no significant intensity fluctuations were detected by monitoring three standard reflections every 150 pieces of data. An empirical absorption correction of the ψ-scan method was applied on both crystals and data with $I > 3\sigma(I)$ were used in the structure refinements. Data processing and all the structure determination calculations were carried out by using the teXsan software package (15).

The space group of SrV_4O_9 and CaV_4O_9 was determined as $P4/n$, being the same as that reported for CaV_4O_9 (5). The unit cell parameters were $a = 8.379(2)$ Å, $c = 5.259(3)$ Å, and $V = 369.2(2)$ Å^3 for SrV_4O_9 and $a = 8.327(3)$ Å, $c = 5.013(4)$ Å, and $V = 347.6(3)$ Å^3 for CaV_4O_9, which were obtained from 2θ reflections of $35.2^\circ < 2\theta < 39.4^\circ$ for SrV_4O_9 and $26.1^\circ < 2\theta < 29.7^\circ$ for CaV_4O_9. The structure of CaV_4O_9 has already been solved by Bouloux and Galy (5) and its atomic coordinates were successfully employed as a starting model. The refinements converged to $R = 0.039$ and $R_w = 0.048$ for SrV_4O_9 based on 826 reflections and $R = 0.037$ and $R_w = 0.040$ for CaV_4O_9 based on 722 reflections. The metal sites of Sr, Ca, and V were confirmed to have essentially full occupancies. Experimental and crystallographic parameters are listed in Table 1 and atomic coordinates and equivalent temperature factors in Table 2. Our crystallographic data of CaV_4O_9 are essentially the same as those given by Bouloux and Galy (5), but we employ our data in the following because our esd's of atomic coordinates are reduced by about 1 order of magnitude.

TABLE 1
Experimental and Crystallographic Parameters of SrV_4O_9 and CaV_4O_9

	SrV_4O_9	CaV_4O_9
Space group	$P4/n$	$P4/n$
a (Å)	8.379(2)	8.327(3)
c (Å)	5.259(3)	5.013(4)
V (Å^3)	369.2(2)	347.6(3)
Z	2	2
D_c (g cm^{-3})	3.916	3.706
Crystal sizes (mm)	$0.35 \times 0.20 \times 0.02$	$0.20 \times 0.15 \times 0.02$
$2\theta_{max}$ (deg)	80	80
Scan width, $\Delta\omega$ (deg)	$1.10 + 0.30 \tan\theta$	$1.00 + 0.30 \tan\theta$
μ (Mo$K\alpha$) (cm^{-1})	120.6	59.7
Trans. coeff. max/min	0.189/0.702	0.454/0.838
No. of reflections ($I > 0$)	1241	1154
No. of reflections ($I > 3\sigma(I)$)	826	722
R_{int}	0.065	0.037
No. of variables	33	33
R/R_w	0.039/0.048	0.037/0.040
$\Delta\rho_{max/min}$ (e/Å^3)	1.13/ −0.99	1.61/ −1.50

RESULTS AND DISCUSSION

Structures of SrV_4O_9 and CaV_4O_9

Figure 1 depicts the structure of SrV_4O_9 having the CaV_4O_9-type structure. As discussed by Bouloux and Galy (5), the structure consists of V_4O_9 layers and interstitial Sr atoms and the V_4O_9 layer is made up of VO_5 square pyramids that are linked by sharing edges. Figure 2 shows a VO_5 square pyramid of SrV_4O_9 and Table 3 lists V–O bond distances and O–V–O bond angles in VO_5 square pyramids and V–V distances between edge-sharing VO_5 square pyramids of both SrV_4O_9 and CaV_4O_9 for comparison. It is said that their values in Table 3 are practically indifferent for both compounds, indicating that the VO_5 square pyramids as well as the V_4O_9 layers are not altered by the change of interstitial atoms from Ca to Sr. The slight expansion of the a axis from CaV_4O_9 to SrV_4O_9 by 0.052 Å is mainly caused by the elongation of V–O(1) and V–O(1)^i distances in Table 3 or more directly O(1)–O(1)^i edges as mentioned below.

TABLE 2
Atomic Coordinates and Equivalent Temperature Factors for SrV_4O_9 and CaV_4O_9

Atom	x	y	z	B_{eq} (Å^2)
		SrV_4O_9		
Sr	0.25	0.25	0.15082(12)	0.721(5)
V	0.15796(6)	0.53784(6)	0.61893(10)	0.594(7)
O(1)	0.0429(2)	0.3566(2)	0.4690(5)	0.66(3)
O(2)	0.1724(3)	0.5096(3)	0.9195(5)	1.23(4)
O(3)	0.25	0.75	0.5	0.68(4)
		CaV_4O_9		
Ca	0.25	0.25	0.1673(2)	0.645(8)
V	0.15845(5)	0.53656(5)	0.62521(9)	0.506(6)
O(1)	0.0445(2)	0.3560(2)	0.4629(4)	0.59(3)
O(2)	0.1769(3)	0.5003(3)	0.9407(4)	0.96(3)
O(3)	0.25	0.75	0.5	0.57(3)

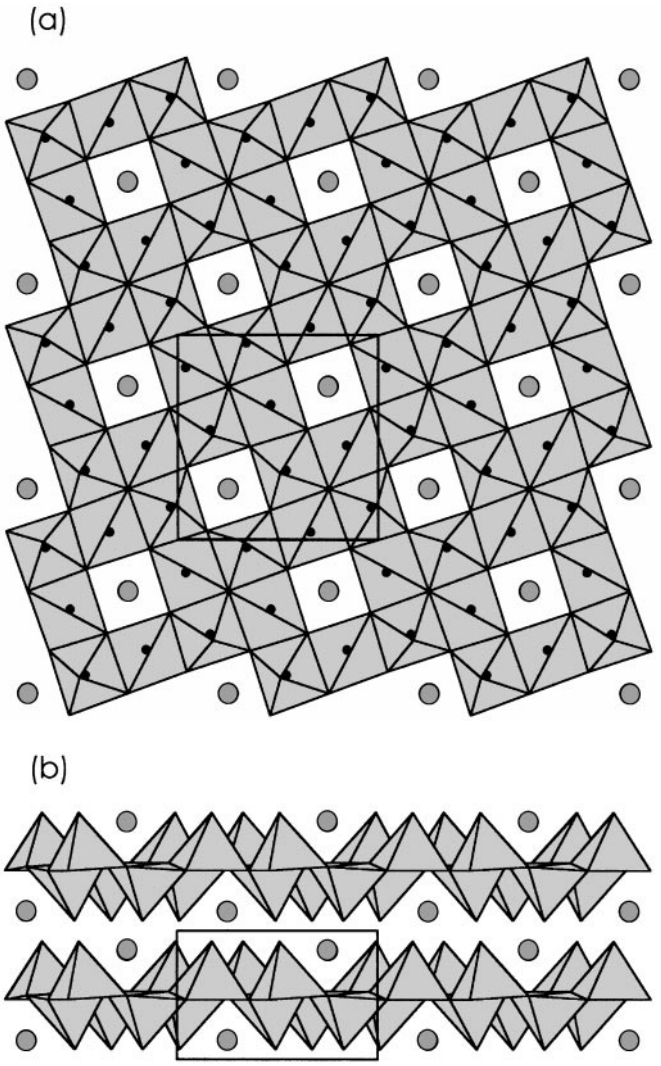

FIG. 1. Crystal structure of SrV_4O_9 viewed along (a) [001] and (b) [010]. Small closed circles denote V atoms in VO_5 square pyramids and large shaded circles denote interstitial Sr atoms.

Interstitial Sr and Ca atoms reside in interlayer space, being coordinated by eight oxygens of the V_4O_9 frameworks forming SrO_8 and CaO_8 polyhedra as depicted in Fig. 3 for a SrO_8 polyhedron: four O(1) bridging oxygens on one side and four O(2) apical oxygens on the opposite side. The Sr, Ca–O bond distances and O(1)–O(1) and O(2)–O(2) edge distances are listed in Table 4. The expansion of bond distances from CaO_8 to SrO_8 polyhedron are 0.141 Å in Sr–O(1) and 0.125 Å in Sr–O(2), as estimated from the increases in ionic radii of 0.14 Å from Ca^{2+} (1.12 Å) to Sr^{2+} (1.26 Å) (16), which results in the elongation of the *c* axis (0.246 Å) from CaV_4O_9 to SrV_4O_9. It is also noted that the increase of the O(1)–O(1) edge by 0.037 Å from CaO_8 to SrO_8 polyhedron causes the elongation of the *a* axis (0.052 Å) and of the V–O(1) bond distances.

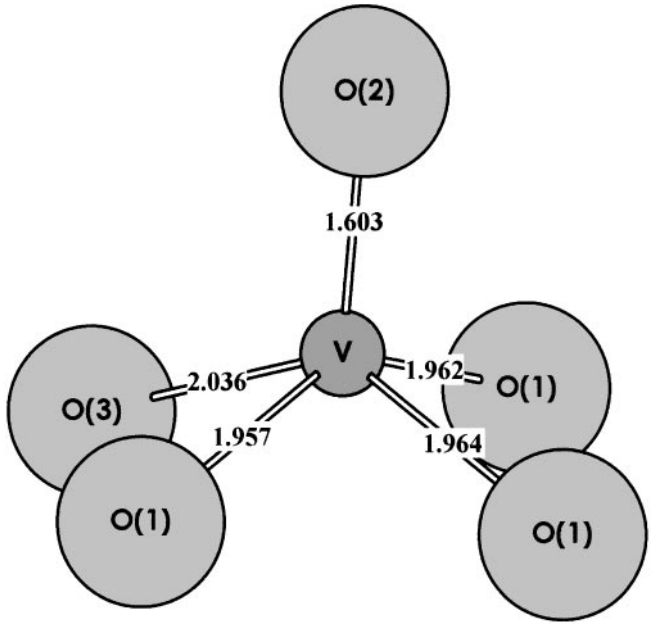

FIG. 2. VO_5 square pyramid of SrV_4O_9. Large and small circles denote O and V atoms, respectively, and numbers indicate V–O bond distances in Å.

Hydrothermal Synthesis of Metastable SrV_4O_9

The equilibrium phase diagram of the Sr–VO_2–V_2O_5 system was studied by Bouloux *et al.* (6), where there exist three strontium vanadium oxides on the SrO–VO_2 side of the triangular diagram, namely, $SrVO_3$, SrV_3O_7, and

TABLE 3
V–O Bond Distances (Å) and O–V–O Angles (deg) of VO_5 Square Pyramids and Edge-Sharing V–V Distances (Å) for SrV_4O_9 and CaV_4O_9

	SrV_4O_9	CaV_4O_9
V–O(1)	1.964(2)	1.955(3)
V–O(1)^{i}	1.962(2)	1.955(3)
V–O(1)^{ii}	1.957(2)	1.963(3)
V–O(2)	1.603(3)	1.617(3)
V–O(3)	2.0362(7)	2.0331(9)
O(1)–V–O(1)^{i}	89.3(1)	88.3(1)
O(1)–V–O(1)^{ii}	80.4(1)	80.7(1)
O(1)–V–O(2)	108.6(1)	108.07(1)
O(1)–V–O(3)^{i}	137.53(9)	136.53(9)
O(1)^{i}–V–O(1)^{ii}	142.23(6)	142.01(6)
O(1)^{i}–V–O(2)	106.3(1)	105.2(1)
O(1)^{i}–V–O(3)	81.73(7)	81.83(7)
O(1)^{ii}–V–O(2)	111.4(1)	112.8(1)
O(1)^{ii}–V–O(3)	81.87(7)	81.66(7)
O(2)–V–O(3)	113.8(1)	115.4(1)
V–V^{iii}	2.996(1)	2.985(2)
V–V^{iv}	3.012(1)	3.009(1)

Note. Symmetry codes: $^{i}y, \frac{1}{2} - x, z$; $^{ii} - x, 1 - y, 1 - z$; $^{iii} - x, 1 - y, 1 - z$; $^{iv}1 - y, \frac{1}{2} + x, 1 - z$.

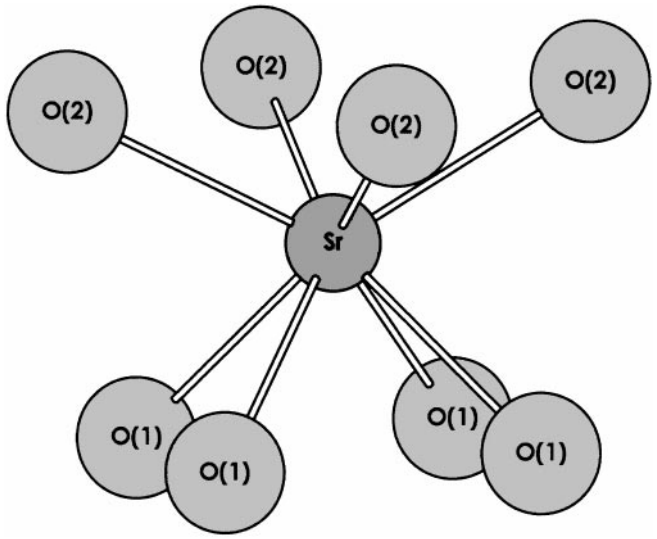

FIG. 3. SrO_8 polyhedron of SrV_4O_9. Large and small circles denote O and Sr atoms.

SrV_5O_{11}. Therefore, SrV_4O_9 is not a stable phase and the formation of SrV_4O_9 by solid-state reactions has never been reported. Actually, the solid-state reaction of $SrVO_3$ and VO_2 in an evacuated silica ampoule at an atomic ratio of $Sr/V = \frac{1}{4}$ yielded biphasic products consisting of SrV_3O_7 and SrV_5O_{11} phases (17), consistent with the phase diagram by Bouloux *et al.* (6). This presents a contrast to the $CaO–VO_2$ system where the CaV_4O_9 phase exists in a stable state, as do the $CaVO_3$, CaV_2O_5, and CaV_3O_7 phases (6).

CaV_3O_7 and CaV_4O_9 adopt similar layered structures with V_3O_7 and V_4O_9 layers, respectively, and both V–O layers are made of VO_5 square pyramids by sharing edges in a similar manner (3, 5). Taking into account that SrV_3O_7 isomorphous with CaV_3O_7 can exist and that CaV_4O_9 is structurally related to CaV_3O_7, SrV_4O_9 isomorphous with CaV_4O_9 could possibly exist in a metastable state. Moreover, we found in the present study that CaV_4O_9 and CaV_3O_7 crystals are hydrothermally synthesized in the $CaCl_2–NaVO_3–(CH_3)_4NCl$ system. The trial of substituting Ca by Sr, namely, the hydrothermal $SrCl_2–NaVO_3–(CH_3)_4NCl$ system, successfully produced SrV_4O_9 crystals in a metastable state. In the hydrothermal $SrCl_2–NaVO_3–(CH_3)_4NCl$ system, reaction temperatures are crucial to obtain SrV_4O_9 crystals which should be well above 300°C: lower reaction temperatures yielded $Sr_{0.5}V_2O_5$ crystals with the δ-type layered bronze structure (6, 18). Unlike the hydrothermal $CaCl_2–NaVO_3–(CH_3)_4NCl$ system, the present $SrCl_2–NaVO_3–(CH_3)_4NCl$ system did not produce SrV_3O_7 crystals that are in a thermodynamically stable state. Trials of hydrothermal synthesis of other thermodynamically stable MV_nO_{2n+1} phases (M = Ca, Sr) such as MVO_3, CaV_2O_5, and SrV_5O_{11} were also unsuccessful.

TABLE 4
Sr,Ca–O Bond Distances (Å) and O–O Edge Distances (Å) of SrO_8 and CaO_8 Polyhedra

	SrO_8	CaO_8
Sr,Ca–O(1)^{i,ii,iii,iv}	2.571(3)	2.430(3)
Sr,Ca–O(2)^{v,vi,vii,viii}	2.576(3)	2.451(3)
O(1)^{i}–O(1)^{iii,vi}	2.760(3)	2.723(3)
O(2)^{v}–O(2)^{vii,viii}	3.211(4)	3.071(4)

Note. Symmetry codes: $^{i}x, y, z$; $^{ii}\frac{1}{2}-x, \frac{1}{2}-y, z$; $^{iii}\frac{1}{2}-y, x, z$; $^{iv}y, \frac{1}{2}-x, z$; $^{v}x, y, z-1$; $^{vi}\frac{1}{2}-x, \frac{1}{2}-y, z-1$; $^{vii}\frac{1}{2}-y, x, z-1$; $^{viii}y, \frac{1}{2}-x, z-1$.

Magnetic Property of SrV_4O_9

As described in the preceding section, CaV_4O_9 has drawn much attention due to its magnetic property originated from V^{4+} ($S = \frac{1}{2}$) ions in a two-dimensional V_4O_9 layer (19). This magnetic system is called a two-dimensional spin system with a spin gap or specifically from a structural viewpoint a spin-plaquette system. As usually found in low-dimensional spin-gap systems, a magnetic susceptibility vs temperature curve of CaV_4O_9 shows a broad maximum around 100 K and a tendency of directing toward zero susceptibility at $T = 0$ K (19). It is of interest of measure a magnetic susceptibility of the new compound SrV_4O_9 with reference to that of CaV_4O_9. Figure 4 shows a magnetic

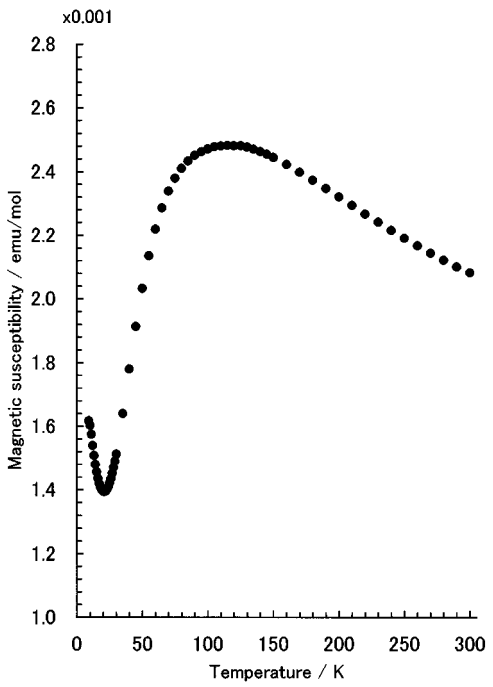

FIG. 4. Magnetic susceptibility vs temperature curve of SrV_4O_9 in an applied field of 0.05 T.

susceptibility vs temperature curve of SrV_4O_9 in an applied field of 0.05 T. The curve clearly exhibits a broad maximum around 100 K just like that of CaV_4O_9, indicating that SrV_4O_9 is also a member of a two-dimensional spin system with a spin gap. Since no significant difference in magnetic susceptibility vs temperature curves between CaV_4O_9 and SrV_4O_9 is detected, their exchange interactions of edge-sharing V–V pairs should almost be equal, as expected from the V–V pair distances in Table 3, exhibiting nearly the same values for both compounds. Quantitative analysis and further experiments to elucidate the magnetic properties of SrV_4O_9 are in progress and the results will be reported elsewhere.

REFERENCES

1. M. Isobe and Y. Ueda, *J. Phys. Soc. Jpn.* **65,** 1178 (1996).
2. Y. Ueda, *Chem. Mater.* **10,** 2653 (1998).
3. J. C. Bouloux and J. Galy, *Acta Crystallogr. Sect. B* **29,** 269 (1973).
4. G. Liu and J. E. Greedan, *J. Solid State Chem.* **103,** 139 (1993).
5. J. C. Bouloux and J. Galy, *Acta Crystallogr. Sect. B* **29,** 1335 (1973).
6. J. C. Bouloux, J. Galy, and P. Hagenmuller, *Rev. Chim. Miner.* **11,** 48 (1974).
7. J. C. Bouloux and J. Galy, *J. Solid State Chem.* **16,** 385 (1976).
8. A. Rabenau, *Angew. Chem. Int. Ed. Engl.* **24,** 1026 (1985).
9. J. Gopalakrishnan, *Chem. Mater.* **7,** 1265 (1995).
10. T. Chirayil, P. Y. Zavalij, and M. S. Whittingham, *Chem. Mater.* **10,** 2629 (1998).
11. Y. Oka, T. Yao, N. Yamamoto, Y. Ueda, and A. Hayashi, *J. Solid State Chem.* **105,** 271 (1993).
12. Y. Oka, S. Sato, T. Yao, and N. Yamamoto, *J. Solid State Chem.* **141,** 594 (1998).
13. JCPDS card No. 27-1065.
14. J. Feldmann and Hk. Müllerbuschbaum, *Z. Naturforsch. B* **50,** 43 (1995).
15. "teXsan for Windows: Crystal Structure Analysis Package," Molecular Structure Corp., The Woodlands, TX, 1997.
16. R. D. Shannon, *Acta Crystallogr. Sect. A* **32,** 751 (1976).
17. M. Isobe and Y. Ueda, private communication.
18. K. Kato, Y. Kanke, Y. Oka, and T. Yao, *Z. Kristallogr.* **213,** 399 (1998).
19. S. Taniguchi, T. Nishikawa, Y. Yasui, Y. Kobayashi, M. Sato, T. Nishioka, M. Kontani, and K. Sano, *J. Phys. Soc. Jpn.* **64,** 2758 (1996).